Passing Ship Effects on Moored Vessels at Piers

Erick T. Huang, PhD, P.E.

Amphibious Systems Division, ESC31
Naval Facilities Engineering Service Center
Port Hueneme, California 93043

Hamn-Ching Chen, PhD

Department of Civil and Ocean Engineering
Texas A&M University
College Station, Texas 77843

Abstract

Passing ships present potential hazards to vessels moored at nearby piers. A Chimera, Reynolds-Averaged Navier-Stokes (RANS) based Computational Fluid Dynamics (CFD) model was used to explore the fluid activities induced by passing ships and their impacts to moored vessels at a complex waterfront next to a navigation channel. This powerful model successfully captured details of ship-ship and ship-pier interactions as they evolve in time, taking into full account the viscous flow physics, exact seafloor bathymetry and basin boundaries, as well as nonlinear couplings between moored ship and pier. Simulation results clearly show the significance of site specific factors to the dynamics of moored vessels induced by passing ships. This paper recapitulates the basic elements of the simulation model and enlightens the general features of passing ship effects as observed by a moored ship. The influences of ship layouts, passing ship speeds, standoff distances of passing ships, and dynamic features of mooring system are discussed.

Introduction

Passing ships engage moored vessels through pressure pulse and wave trains. These mechanisms are rather complicated in confined waters. Traditional methods based on field and laboratory observations often fall short of catching the influences of site specific factors relevant to irregular ship basins, sea floors, and pier facilities. At shallow water, the effects of vorticity and viscosity may be critical to ship-ship and ship-pier interactions. These factors, which are normally left out from potential-theory base codes, are rigorously treated in modern viscous CFD codes. Recent advances in hydrodynamic theories and computation power drastically enhance the reliability and efficiency of high level CFD simulators for design applications. NFESC, in conjunction with Texas A&M University, had successfully applied this advanced tool to several major projects through a hybrid simulation model, FANSMA code. Examples could be found in Chen et al. (2000) and Huang and Chen (2003). This sophisticated code comprises a powerful fluid solver, FANS[1], and a three-dimensional rigid-body motion tracer, COSMA[2], of NFESC. FANS is a typical unsteady, incompressible, three-dimensional fluid solver originated by Prof. H. C. Chen of Texas A&M University based on RANS theory. Performance of this code had been carefully validated with field and laboratory tests.

Passing ship effects as observed by a moored vessel at pier varies with a wide variety of physical parameters, including (a) hull characteristics of moored and passing ships, (b) speed, heading, and location of passing ships, (c) geometries of ship basins, (d) orientation of moored ship, and (e) dynamic properties of mooring systems. Besides, these factors are not independent. The effect due to a specific parameter may change greatly as other parameters vary. Since the

[1] FANS stands for Finite Analytical Navier Stokes code.
[2] COSMA stands for Compound Ocean Structure Motion Analyzer.

flow activities at a true waterfront comprising irregular ship basins are rather complex, a parametric study was first conducted in a straight navigation channel of constant water depth to explore the relative importance of the dominating factors. Findings were used to guide a complete simulation at a real waterfront and to assist data processing of the simulation results. Basic elements of the simulation model and important features of passing ship effects at the waterfront are illustrated through this exercise. For brevity, this paper only presents the roles of passing ship speeds, lateral distances between passing and moored ships, and properties of mooring system. Theoretical backgrounds of the model and experimental justifications are also briefly summarized for references.

Theoretical Background

The transient flow induced by passing ships was addressed with the Chimera RANS method of Chen, Chen and Davis (1997) and Chen, Chen and Huang (1996). This method has been used for time-domain simulation of complex free surface flow induced by berthing ships undergoing simple lateral motion. Results successfully captured many important features of the transient flow around the ships. This method solves the mean flow, including pressure and velocity fields, and turbulence quantities. A chimera domain decomposition scheme was employed to achieve a close fit of irregular boundaries at extreme efficiency ant to accommodate the relative motions between different grid blocks. The governing equations were formulated in an earth-fixed reference frame and transformed into general curvilinear, moving coordinate systems as follows.

Consider the non-dimensional Reynolds-Averaged Navier-Stokes equations for incompressible flow in orthogonal curvilinear coordinates $(x^i, t) = (x^1, x^2, x^3, t)$

$$U^i_{,i} = 0 \tag{1}$$

$$\frac{\partial U^i}{\partial t} + U^j U^i_{,j} + \overline{u^i u^j}_{,j} + g^{ij} p_{,j} - \frac{1}{\mathrm{Re}} g^{jk} U^i_{,jk} = 0 \tag{2}$$

where U^i and u^i represent the mean and fluctuating velocity components, and g^{ij} is conjugate metric tensor. t is time, p is pressure, and Re = $U_0 L / \nu$ is the Reynolds number based on a characteristic length L, a reference velocity U_0, and the kinematic viscosity ν. Eq. (1) represents the continuity equation and Eq. (2) represents the mean momentum equation. The equations are written in tensor notation with the usual summation convention assumed. The subscripts, $_{,j}$ and $_{,jk}$, represent the covariant derivatives.

The Reynolds stress tensor $\overline{u^i u^j}$ are related to the corresponding mean rate of strain through an isotropic eddy viscosity ν_t as recommended by Chen and Patel (1988).

$$-\overline{u^i u^j} = 2\nu_t S^{ij} - \frac{2}{3} g^{ij} k \tag{3}$$

with $$S^{ij} = \frac{1}{2}\left(g^{ik} U^j_{,k} + g^{jk} U^i_{,k}\right); \qquad k = \frac{1}{2} g_{ij} \overline{u^i u^j} \tag{4}$$

where S^{ij} represent the contravariant components of the rate-of-strain tensor, and k is the turbulent kinetic energy. Substituting Eq. (3) into Eq. (2) yields:

$$\frac{\partial U^i}{\partial t} + U^j U^i_{,j} + g^{ij}\left(p + \frac{2}{3} k\right)_{,j} - 2\nu_{t,j} S^{ij} - \frac{1}{R_u} g^{jk} U^i_{,jk} = 0 \tag{5}$$

The quantity $1/R_u = 1/\mathrm{Re} + \nu_t/\sigma_u$ represents the effective eddy viscosity. In the fully turbulent flow regions away from the solid walls, the standard *k*-ε equation is employed to solve the transport equations for turbulent kinetic energy *k* and its dissipation rate ε:

$$\frac{\partial k}{\partial t} + U^j k_{,j} - \left(\frac{1}{R_k} g^{ij} k_{,j} \right)_{,i} - G + \varepsilon = 0 \tag{6}$$

$$\frac{\partial \varepsilon}{\partial t} + U^j \varepsilon_{,j} - \left(\frac{1}{R_\varepsilon} g^{ij} \varepsilon_{,j} \right)_{,i} - C_{\varepsilon 1} \frac{\varepsilon}{k} G + C_{\varepsilon 2} \frac{\varepsilon^2}{k} = 0 \tag{7}$$

where the eddy viscosity, ν_t, and the production term, *G*, are given by:

$$\nu_t = C_\mu \frac{k^2}{\varepsilon}; \quad G = 2\nu_t g_{im} g_{jn} S^{ij} S^{mn} \tag{8}$$

The effective viscosities in Eqs. 6 and 7 are taken as $1/R_k = 1/\mathrm{Re} + \nu_t/\sigma_k$, and $1/R_\varepsilon = 1/\mathrm{Re} + \nu_t/\sigma_\varepsilon$, respectively.

The dissipation rate in the near wall region is determined from the turbulent kinetic energy and the dissipation length scale ℓ_ε to account for the wall effects:

$$\varepsilon = \frac{k^{3/2}}{\ell_\varepsilon}; \quad \ell_\varepsilon = C_\ell y \left[1 - \exp(-R_y / A_\varepsilon) \right] \tag{9}$$

Using this relationship, the turbulent kinetic energy can be determined from Eq. 6 with the following eddy viscosity distribution:

$$\nu_t = C_\mu \sqrt{k \ell_\mu}; \quad \ell_\mu = C_\ell y \left[1 - \exp(-R_y / A_\mu) \right] \tag{10}$$

The constants C_ℓ, A_μ, and A_ε are given in Chen and Patel (1988) and chosen to yield a smooth distribution of eddy viscosity between the two regions.

The free surface boundary conditions consist of one kinematic and three dynamic conditions. In Cartesian coordinates, the kinematic free surface boundary conditions can be expressed as

$$\frac{D\eta}{Dt} = \frac{\partial \eta}{\partial t} + U \frac{\partial \eta}{\partial x} + V \frac{\partial \eta}{\partial y} - W = 0; \text{ on } z = \eta(x, y) \tag{11}$$

where η is the free surface wave elevation and (*U, V, W*) are the longitudinal, transverse, and vertical velocity components on the free surface z = η(*x, y*). For general viscous fluid flows, the dynamic conditions represent the continuity of stresses on the free surface. When the surface tension and free surface turbulent boundary layer are neglected, a set of simplified dynamic boundary conditions can be employed by simply extrapolating the velocities from the inner fluid domain and maintain constant total pressure on the free surface. Since the RANS equations solve only the dynamic pressure *p*, the dynamic boundary condition for constant total pressure can be expressed as follows:

$$p = \frac{\eta}{Fr^2} \tag{12}$$

where $Fr = U_o / \sqrt{gL}$ is the Froude number based on the ship length *L*.

The equation of continuity and the transport equations for mean flow and turbulence quantities ma be transformed into body-fitted coordinate system using the partial transformation described in Chen, Patel and Ju (1990).

In the present chimera RANS method, the solution domain is first decomposed into a number of computational blocks. The body-fitted numerical grids for the ship and the fluid domain are generated separately with the ship grid blocks completely embedded in the fluid grids as illustrated by the example in Figure 1. The ship grids are allowed to move with a prescribed velocity relative to the fluid grids in arbitrary combinations of translational and rotational motions. The PEGSUS program (Suhs and Tramel, 1991) is employed every time step to determine the interpolation information for linking grids across different blocks. The overall solution procedure consists of an outer loop over time and an inner loop that iterates over the blocks of the grid. The discretized equations for pressure, velocity, and turbulence quantities form a system of tri-diagonal matrices that was solved using an iterative scheme.

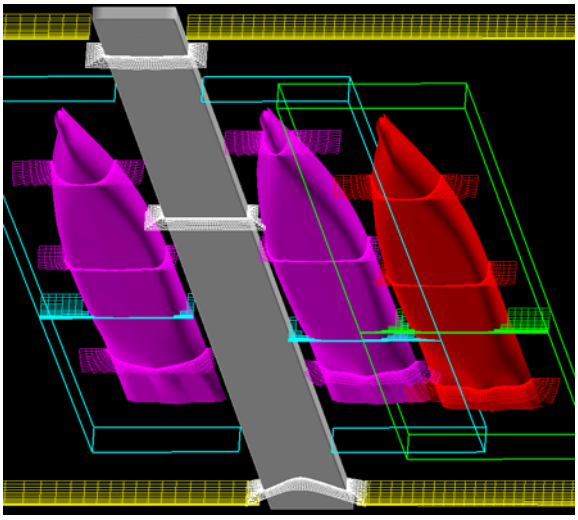

Figure 1 Example of Chimera grids

In order to predict the responses of moored ships and their feedback to the ambient flows, the FANS code was coupled with a six-degree-of-freedom motion analyzer, COSMA, developed by Huang (1990). Coupling forces on fenders and mooring lines may be assessed based on the relative motion between moored ships and piers. The equation of motion implemented in the COSMA can be written in the following general form:

$$[M+a]\{\ddot{X}(t)\}+[b]\{\dot{X}(t)\}+[K+C]\{X(t)\}=\{f(t)\} \tag{13}$$

in which [M] represents the generalized inertia matrix, [a] is the hydrodynamic mass matrix, [b] is the hydrodynamic damping matrix, [K] is the hydrodynamic restoring force matrix, [C] is the restoring forces due to coupling members, {X(t)} is the generalized displacement vector, and {f(t)} is the generalized external excitation force vector.

The present method solves the unsteady RANS equations at each grid node for the transient velocity and pressure fields induced by the berthing ships. Therefore, the hydrodynamic force vector $\{F_h(t)\}$ can be readily obtained by a direct integration of the surface pressure and shear stresses over the wetted hulls of the floating structures. Since the hydrodynamic forces $\{F_h\}$ includes both the added mass and damping forces, Equation (13) can be rearranged in a convenient form as follows:

$$[M]\{\ddot{X}(t)\}+[K+C]\{X(t)\}=\{F_h(t)\} \tag{14}$$

For ship induced flows, the chimera RANS method was employed first to calculate the transient flow field and the associated hydrodynamic forces $\{F_h(t)\}$. The COSMA program was then used to solve the displacement vector {X(t)} from Equation (14). Once the new ship position and the corresponding fender deflection are determined, the numerical grids can be updated by following the ship motion. A more detailed description of the COSMA program and the coupled RANS / COSMA coupling method is given in Huang and Chen (2003) and Chen et al. (2000).

Validation

The performance of the FANSMA code had been validated with a series of field and towing tank tests. This simulation model consistently reproduced field and laboratory measurements at great accuracy. Two most important evidences are recaptured here for references. One is a towing tank observation of wave-induced water particle velocity and vorticity fields around the corner of a partially submerged rectangular cylinder in regular wave trains as illustrated by Figure 2. Figure 3 shows comparisons of the

measured and simulated free surface elevations, velocity vectors, and phase-averaged vorticities at 8 different phases over one wave period. More details of this test were described in Chen et al. (2002).

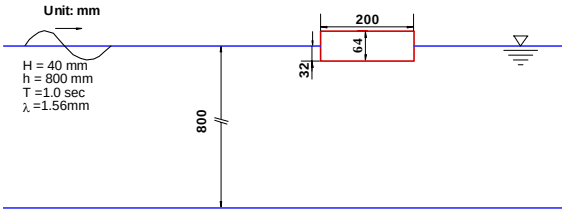

Figure 2. Schematic for fixed-barge experiment.

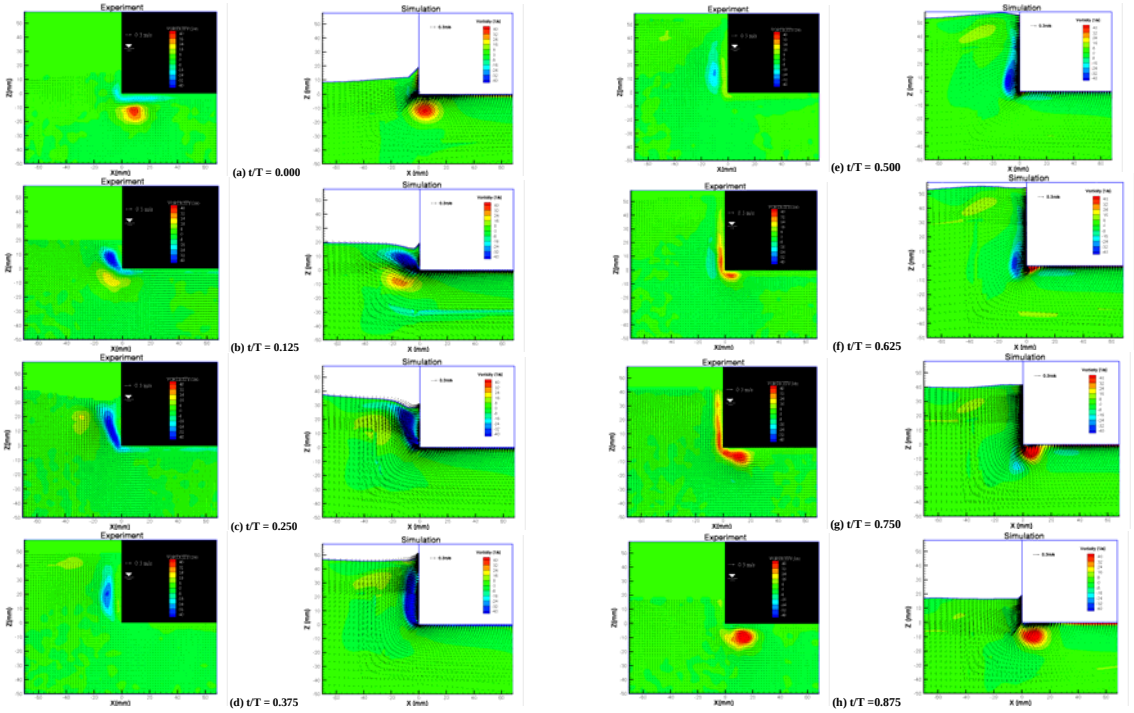

Figure 3. Comparison of measured (left) and calculated (right) velocity vectors, and vorticity

It is clearly seen that the computed free surface elevations are in close agreement with the corresponding measurements. Furthermore, the locations and sizes of the computed vortices were also accurately predicted. The vorticities are mainly created around the barge corners due to flow separations induced by the wave motion. At t/T = 0, the free surface is roughly leveled with the wave trough and begins to move upward. As the water level rises, the fluid was pushed from the barge bottom towards the front face of the barge. Due to the strong upward wave motion, the flow separates from the barge corner and a strong clockwise vortex was formed along the front face of the barge as seen in Figures 3(b)-(d). At t/T = 0.5, the free surface is close to its crest value and the water level begins to drop. When the flow reverse its direction, the clockwise vortex decay gradually while an elongated counterclockwise vortex was formed along the sidewall as seen in Figure 3(e)-(f). At t/T = 0.75 and 0.875, the fluid continued to move downward into the barge bottom. The downward fluid motion has led to the formation of a large counterclockwise vortex with strong flow separation around the sharp corner of the barge.

The other is a field measurement of berthing forces and flow patterns induced by a docking ship as shown in Figure 4. During the test a ship was docking against two instrumented fenders where the berthing forces were monitored. An array of eight current meters (see the top right insert) was placed

under the path of docking ship to record the ship induced currents throughout the process. More details of this test were described in Chen et al. (2000), respectively.

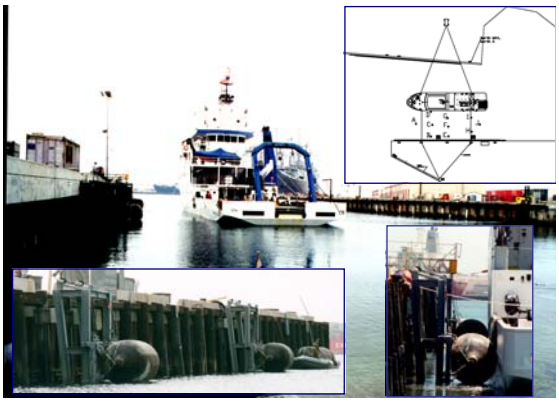

Figure 4 At-sea test of ship docking process

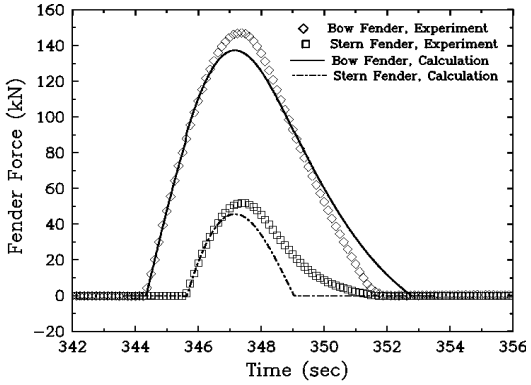

Figure 5 Fender forces

FANSMA precisely predicted both bow and stern fender forces observed throughout the compression cycle. The model predicted slightly lower peak loads and somewhat earlier rebound of the stern fender. The discrepancy is most likely due to certain nonlinear characteristics of the fender piles, which were not fully implemented in this model. Figure 6 further fortifies the credibility of this model with the velocity field observed by the current meter array at the sea floor as shown in the top right insert in Figure 4. FANSMA consistently captured the mean flow (solid lines) at great accuracy. The differences shown in Gage J were attributed to incorrect gage position. However, these minor discrepancies should not discount the credibility of this powerful code and its potentials to be a powerful design tool.

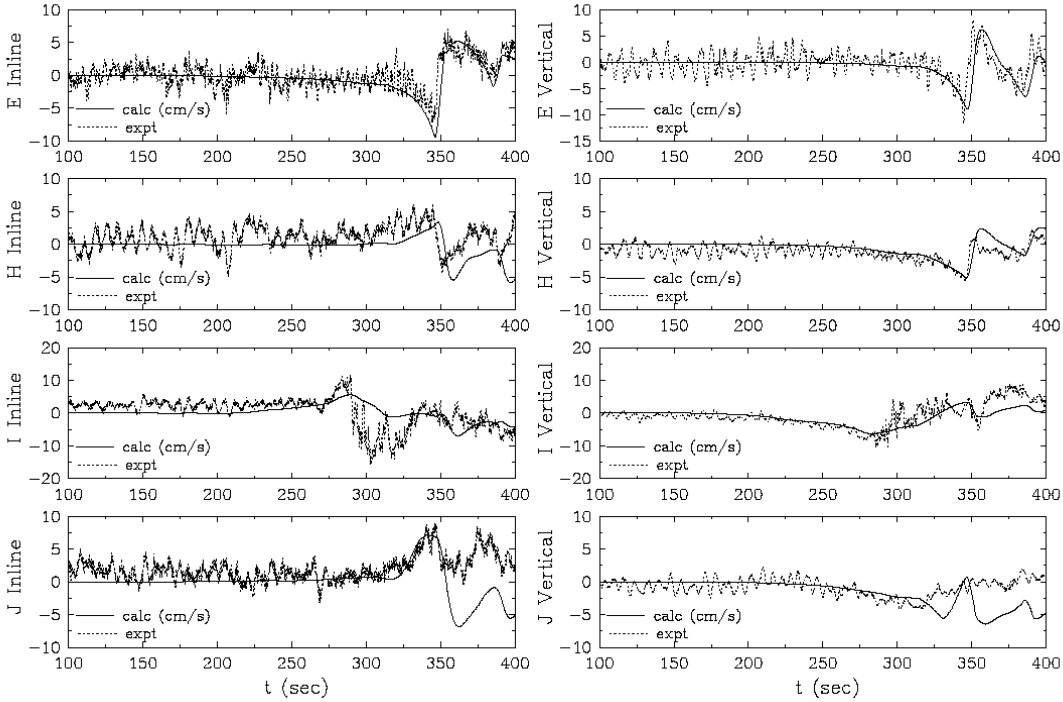

Figure 6 Comparison of ship induced velocities at various locations

Computation Domain and Model Layout

A generic model comprising three ships of the same hull in a straight channel depicted by Figure 7(a) was used to demonstrate the nature of passing ship effects observed by a moored ship in confined water. Two hulls in the middle of channel represent the inbound and outbound traffic and a third ship situated along the near edge of the channel represents a moored ship held to an open pier through mooring lines and fenders as shown in Figure 7(b). The reference coordinates are also shown in the same figure with the *z*-axis pointing out of the page. The motion, forces, and moments presented in this paper are consistent with this reference. This idealized model simplifies the flow activities and thus offers a better chance to track the performance of each parameter. In fact, this model was further reduced to one passing ship in many cases whenever couplings between passing ships are not the center of focus. Findings from this model provide basis to interpret the highly intricate flow activities at complex waterfronts.

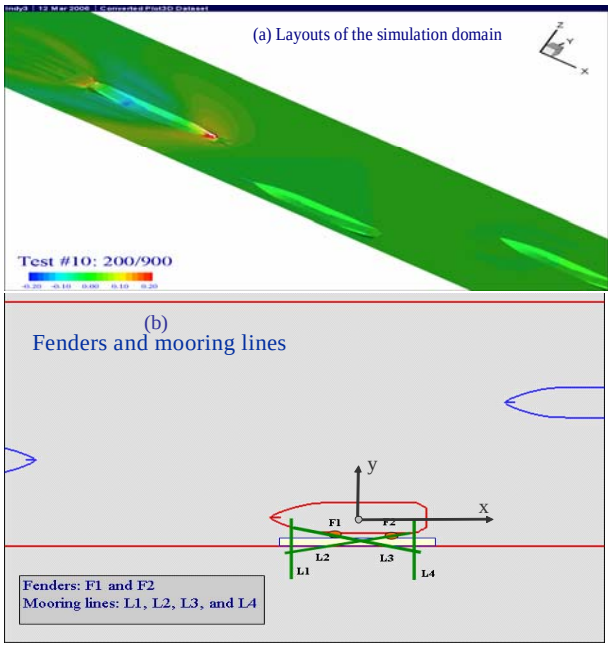

Figure 7 Computation domain and ship layouts

Results

This study was conducted over a matrix of parameters including ship layouts, ship speeds, separation distances between ships, drift angles, and characteristics of mooring system. The influence of each parameter and interactions between selected parameters were analyzed. For brevity, this paper presents only the effects of ship layouts, ship speeds, and separation distances between ships. The role of mooring lines and fenders can also be observed through these cases.

Passing ship layouts

Traffic situation in the channel decides the flow patterns and the consequent passing ship effects. Traditional methods account multiple ship effects by simply adding the contributions of each individual vessel in scene. The effects of ship-ship couplings among the traffic ships are often overlooked. A simple test was conducted to explore the sensitivity of ship-ship couplings and thus to confirm the feasibility of superposition assumption. A base case was established by letting two passing ships approach head-on and eventually meet near the bow of moored ship. Two other cases were repeated with either ship cruising in the same scene alone. Figure 8 is a movie clip comparing the moored ship responses in these three cases. Each row in the move frame presents the moored ship responses to a specific passing ship layout as labeled. The surge, sway, and yaw motions as perceived from the port side, bow and keel (fish eye view) are shown in respective columns. The bottom frame shows the instant locations of passing ships for the case in row three. The same for other cases may be taken from the appropriate ship in the same frame. This movie may be actuated by clicking on the figure if the embedded file is available. Otherwise, the associated motion responses are summarized in Figure 9. It can be seen that the base case does not always produce the largest excursion in this specific case. Either passing ship alone may excite the moored ship more extensively at certain stages. A good example can be seen with the sway motion when traffic ships pass the moored ship (between 15 to 25 seconds). The base case indeed migrates between two other cases with one ship alone. This is a clear sign of hydrodynamic couplings between passing

ships. The influence is illustrated in Figure 10 by comparing the forces predicted by direct simulation (denoted by "couplings") to the results obtained by superposition (denoted by "superposition"). Figure 10(a) indicates that the superposition results trace closely the predictions by direct simulation in surge force (Fxx), however, deviates substantially in sway forces (Fyy) and yaw moments (Rzz). This result should not be a total surprise, since the flow field induced by an individual ship alone does not recognize the constraints posted by the other ship. The process of superposition has no mechanism to implement the additional information at all. It can be anticipated that ship-ship couplings will be more pronounced for larger hulls in shallower water. This explains why traditional superposition assumption works well for surge mode. As a ship is normally well streamlined and presents a small cross section along its long axis, it posts the least interfere to the other ship. In fact, there is little basis to superpose motion responses if the driving forces are not justified, Figure 10(b).

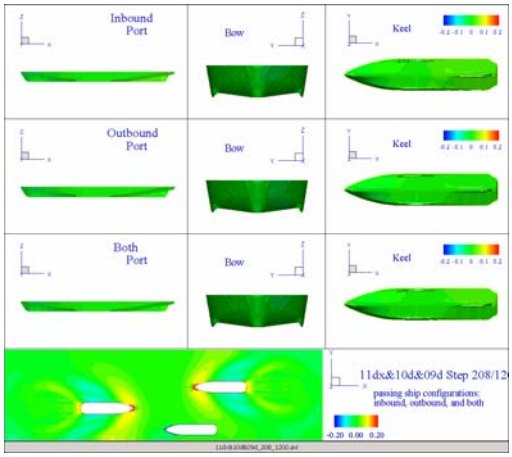

Figure 8 Motion responses (effect of ship layouts).

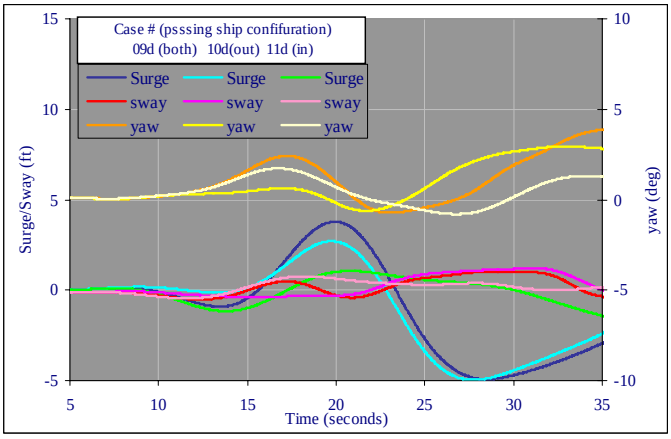

Figure 9 Motion histories (effect of ship layouts).

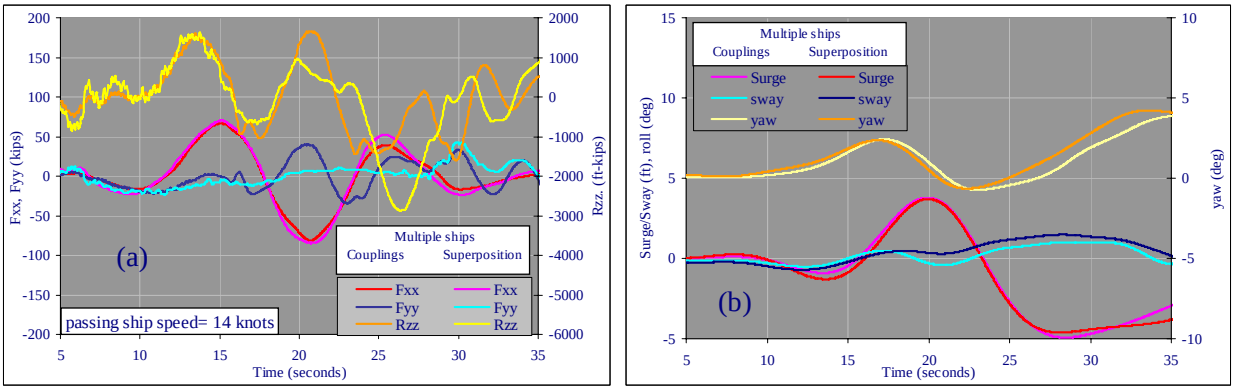

Figure 10 Evaluation of the superposition assumption (a) fluid forces and (b) motion responses

Separation distance

Ships in navigation channel close to pier facilities are usually held to low speeds. Under this circumstance, the passing ship effects are transmitted primarily through pressure impulses. Effect of surface waves is negligible. While pressure impulse normally decays exponentially away from ship hull in open water, its behaviors are not as clear in confined shallow waters. A series of simulations was

conducted to verify the sensitivity of passing ship effects as a function of stand-off distances. For clarity, this test series considered only one passing ship cruising at a constant speed of 14 knots along a straight course. Three standoff distances equal to 0.4, 0.6, and 0.8 times of the ship length from the moored ship were tested. Figure 11 summarizes the resulting fluid forces on the moored ship. The horizontal axis represents the longitudinal distance between the midships of these two ships. A value of zero indicates that two ships are abreast. Figure 11(a) compares the exciting forces induced by traffic ships on a moored ship held fixed in its equilibrium position. No radiation force is involved in this case. Again, surge forces decrease consistently as the standoff distance increases. The trends of sway force and yaw moment are far more complicated. These two force components observe a similar decay trend initially but reverse the trend as the traffic ship is passing by. This might have to do with pressure bouncing back and forth between ship hulls and channel walls. Figure 11(b) presents the same for a moored ship under moderate mooring. The fluid forces in this case include passing ship excitations shown in Figure 11(a) and the radiation forces in response to the moored ship movement. Surge forces, which is least influenced by the radiation forces, remain intact. Sway force and yaw moment, on the other hand, retain the overall shape but substantially reduced in magnitudes. These results are reasonable because the radiation forces are supposed to increase with ship displacements but oppose in direction. As a result, the radiation forces tend to cancel the exciting forces. The radiation forces are obviously the most pronounced in sway and yaw. Figure 12 compares the motion responses of the moored ship induced by passing ship at various standoff distances. The time histories of surge, sway, and yaw motions are captured in Figure 13.

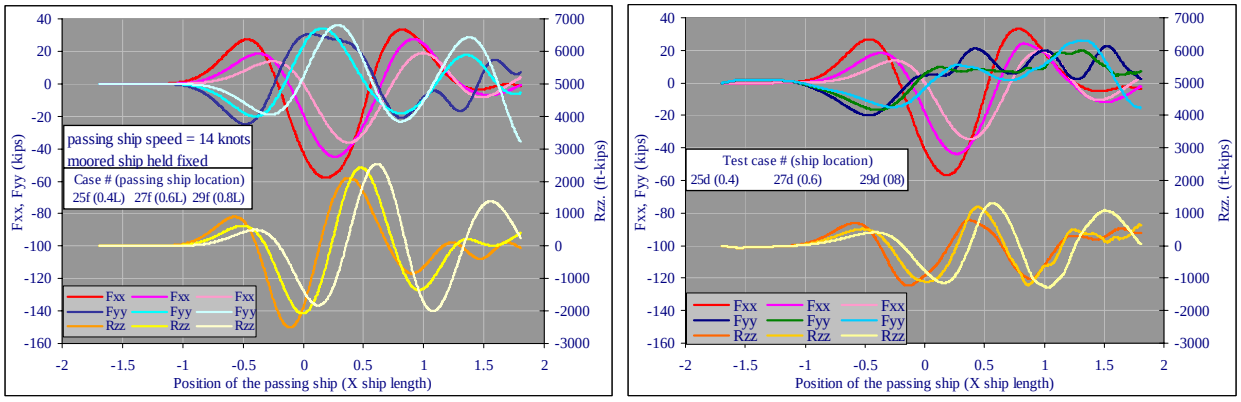

Figure 11 Fluid forces on the moored ship: (a) passing ship excitations, (b) net forces

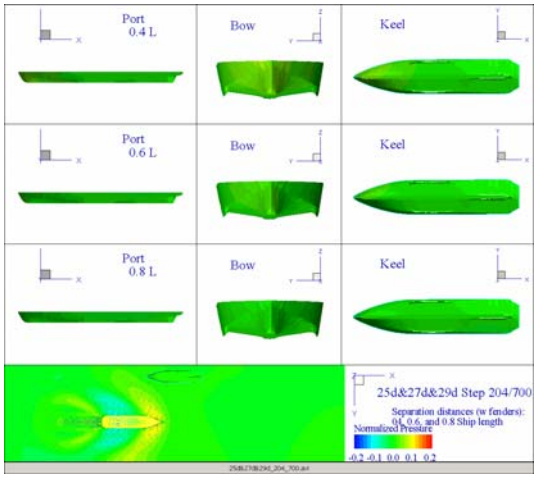

Figure 12 Motion responses (effect of standoff distance)

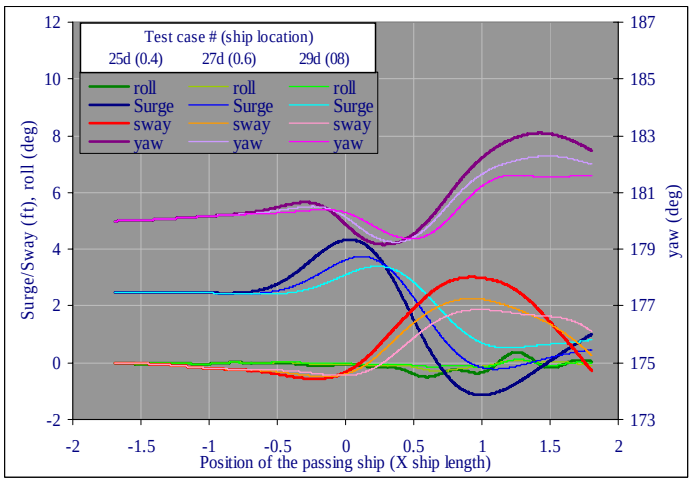

Figure 13 Motion histories (effect of standoff distance)

Speed of passing ships

Pressure impulses in open waters in general increase proportionally to the ship speed square. For instance, the pressure intensity is expected to increase by four folds if the passing ship doubles its speed. A simulation series was conducted to test the feasibility of this assumption in confined water. This test series considered one passing ship at speeds of 7, 10, and 14 knots. These three speeds are separated roughly by a factor of $\sqrt{2}$ such that the consequent fluid forces are expected to separate by a factor of 2. Other parameters remain constant throughout the test series. The passing ship maintains a straight course down the channel at a distance of 0.4 times of the ship length away from the moored ship. Mooring lines and fenders are set to a moderate stiffness for the size of the model ship. Figure 14 compares motion responses of the moored ship. Each row presents the responses to a specific passing ship speed as labeled. Figure 15 captures the histories of: (a) fluid forces and (b) motion excursions of the moored ship as well as (c) the fender loads and (d) mooring line tensions, respectively. The horizontal axis shows the longitudinal distance between two ships. A value of zero indicates that two ships are abreast. Note that the fluid forces presented here are the net forces, which include the radiation forces resulting from ship movement. Figure 15(b) is in fact the motion histories of the moored ship illustrated in Figure 14.

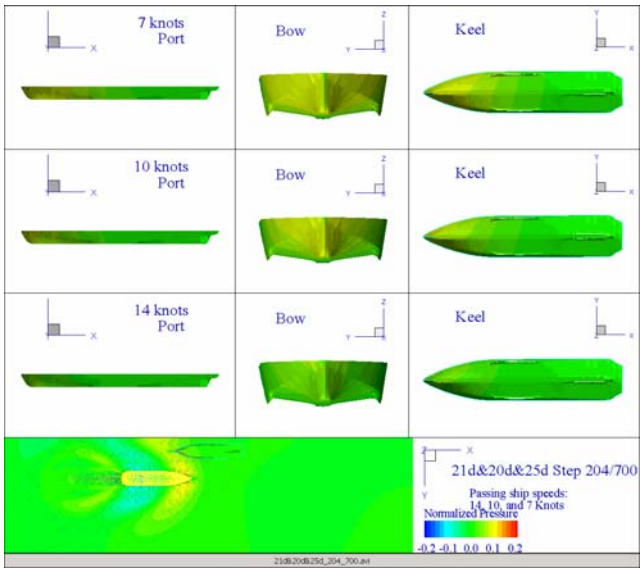

Figure 14 Motion responses (Effects of ship speeds)

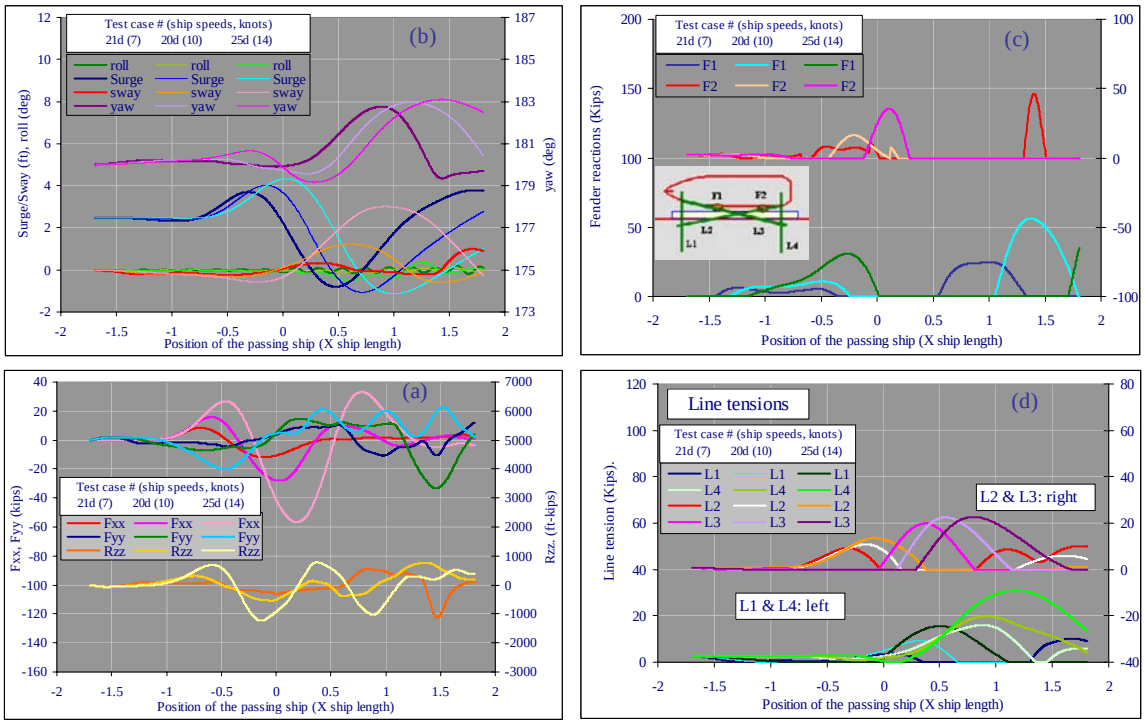

Figure 15 Passing ship effects as a function of ship speeds.

It is interested to note from Figures 15 (a) and (b) that the moored ship feels slower passing ship sooner (in term of ship location), despite that pressure waves travel at sound speeds. The fluid forces sent by a slower ship appear and reach the peak sooner than those of a faster ship. Changing ship speed changes the phase and magnitude of the fluid forces. The trend is more pronounced in motion responses.

In fact, Figure 15(a) does not support the assumption of speed square in confined water. While surge forces generally follow this rule, sway forces and yaw moments, however, increase substantially stronger than the rule indicates. However, this set of data might be misleading as the forces are depending on ship motion, which reflects the influence of mooring restraints. Figures 16 and 17 clarify these doubts by eliminating mooring restraints. Figure 16 presents the fluid forces on a fixed ship, comprising the exciting forces produced by the passing ship alone. Figure 17 presents the forces on an unrestrained ship, representing the total fluid forces including the radiation component. The differences between these two cases are obviously the radiation forces. Despite the obvious distinction in their motion, both sets confirm the trend described by Figure 15(a) as ship speeds increase.

Besides, it can be seen that there is hardly any difference in surge forces, a sign of negligible radiation forces. The radiation forces in sway and yaw, on the other hand, can be as significant as 50% of the corresponding excitation forces. This raises a legitimate concern in the accuracy of radiation forces transverse to ship axis. It is well known that cross currents induce severe flow separations or recirculation around sharp edges of a ship. A full interpretation of this erratic flow requires detailed viscosity and vorticity information of the flow. A high performance viscous flow solver is mandated to properly capture the radiation forces. Improper driving forces may severely distort the motion performance of a ship and lead to unrealistic fender and mooring loads.

Motion displacements, on the other hand, increase only slightly as the ship speed doubles. A slower passing ship seems more effective in moving the moored ship. However, motion responses are heavily influenced by the dynamic characteristics of mooring restraints. The resulting fender loads and mooring tensions follow neither motion history nor force history in any mode.

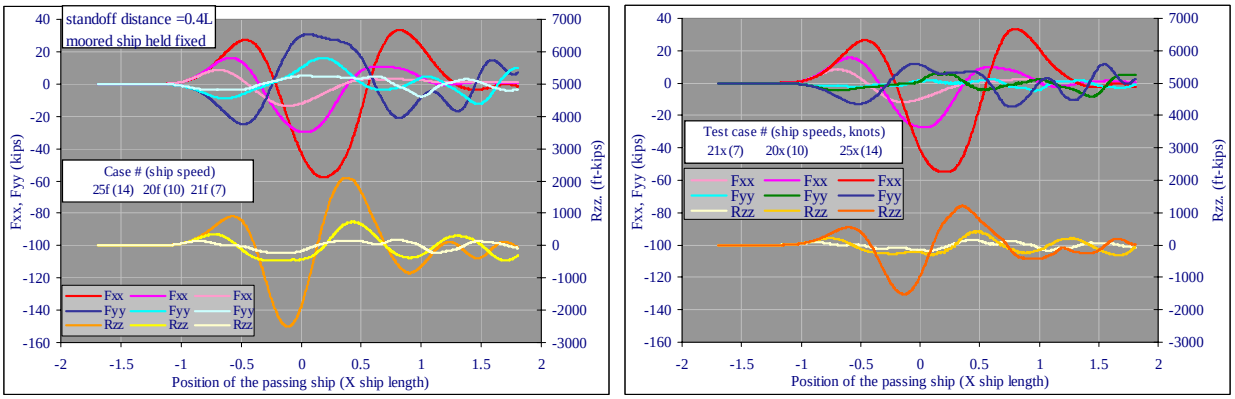

Figure 16 Fluid forces on the moored ship: (a) fixed, (b) unrestrained

Field application

FANSMA code is further tested for its performance to handle site specifics at a nature waterfront as shown in Figure 17. This waterfront comprises a series of ship basins along a straight channel. The opposite side of the channel is attached to a wide open water of shallow depth. The entire simulation area measures roughly 10,000 feet long by 5000 feet wide. Two hulls in the channel represent the outbound

and inbound ships in their respective lanes. The outbound ship is closer to the waterfront than the inbound ship. A third ship is moored in one of the ship basins with its bow heading nearly perpendicular into the channel. A shoal basin is situated near the port side of the moored ship. This test considered three traffic conditions: (a) inbound ship alone, (b) outbound ship alone, and (c) both ships in the channel.

The analysis is currently in process. However, results to date positively confirmed several critical functions of the FANSMA code required to handle large water domains with multiple ships in arbitrary motions. The Chimera domain decomposition scheme facilitates a sure means to closely address highly complex geometries of a nature waterfront. The benefit is clearly illustrated in the process of capturing the sheltering shadow created by a shoal on the port side of the moored ship. Figure 18 presents four snap shots of pressure contours on sea floor around the moored ship when the outbound ship went by the shoal. It can be seen the region behind the shoal water is relatively calm. An exact sea floor bathymetry is required to catch meaningful result of this effect.

Figure 19 is a movie clip summarizing the results of case (c). The six frames appear in the movie illustrate the pressure fields induced by passing ships (middle row), and motion responses of the moored ship from three perspective angles (top row), pressure fields around the moored ship (bottom left), and the overall view of the simulation area (bottom right), respectively. Figure 20 compares the fluid forces on the moored ships observed in three test conditions. It is seen that the total fluid forces on the moored ship are mainly contributions of the outbound (near) ship. However, the presence of inbound ship delays the maximum force by as much as 40 seconds or one ship length. This is a result of the strong coupling between the passing ships. The positive bow pressure of the inbound ship tends to cancel the negative shoulder pressure of the outbound ship. Consequently, the full effect of outbound ship does not display until two ships are sufficiently separated. Besides, the strong oscillations of fluid forces observed in the case of rectangular channel disappear as expected, because the pressure impulses are now propagating out of the navigation channel. All observations so far receptively support the performance of FANSMA code for field applications.

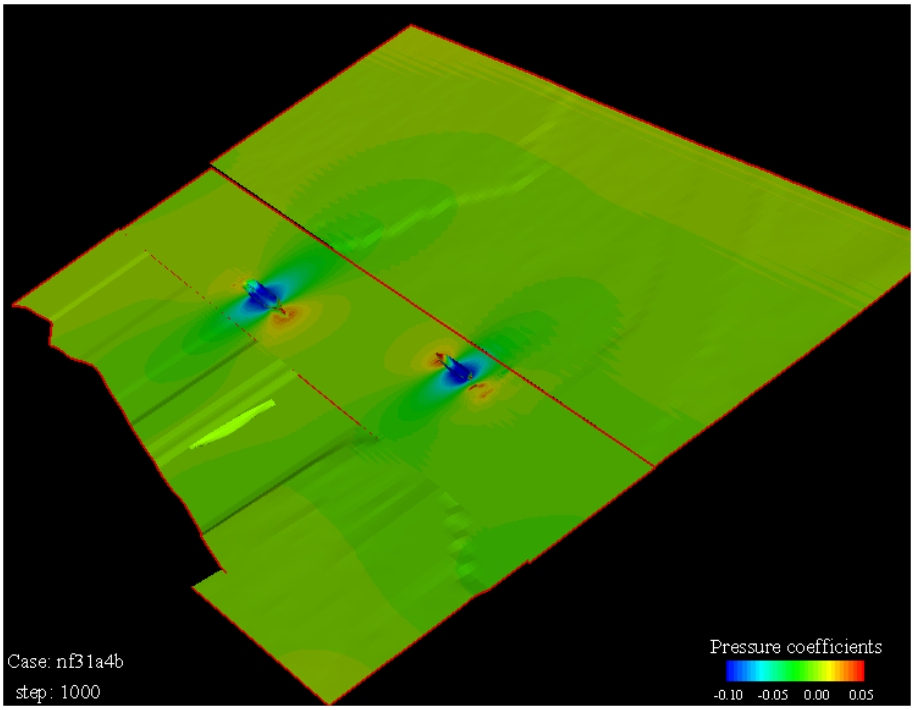

Figure 17 Simulation domain and ship layouts at a nature waterfront

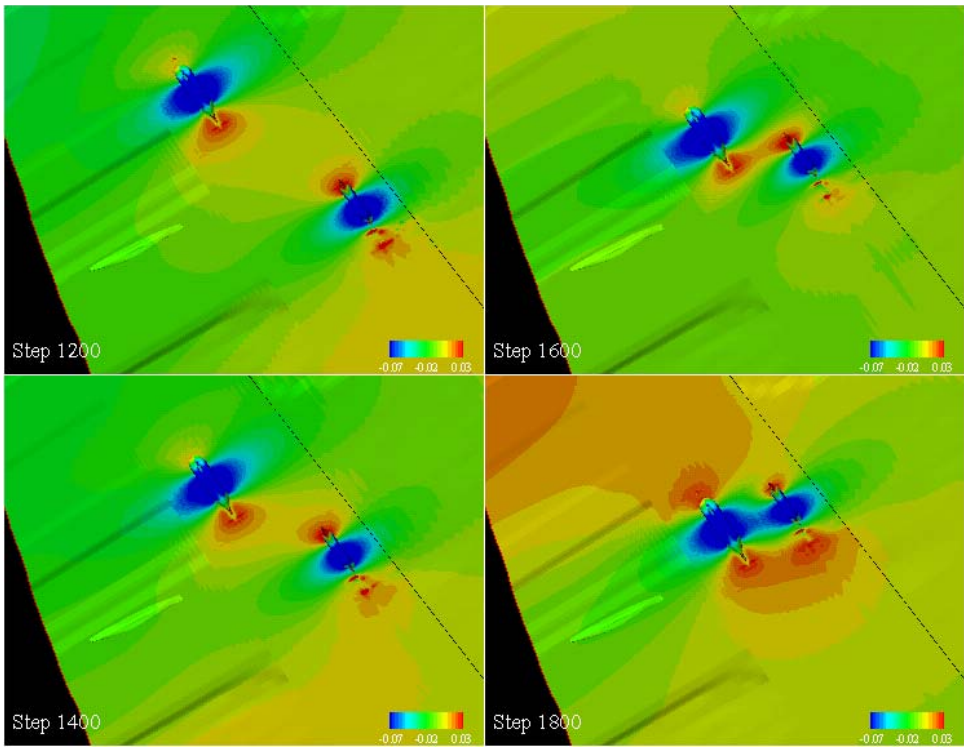

Figure 18 Shelter effects of shoal water

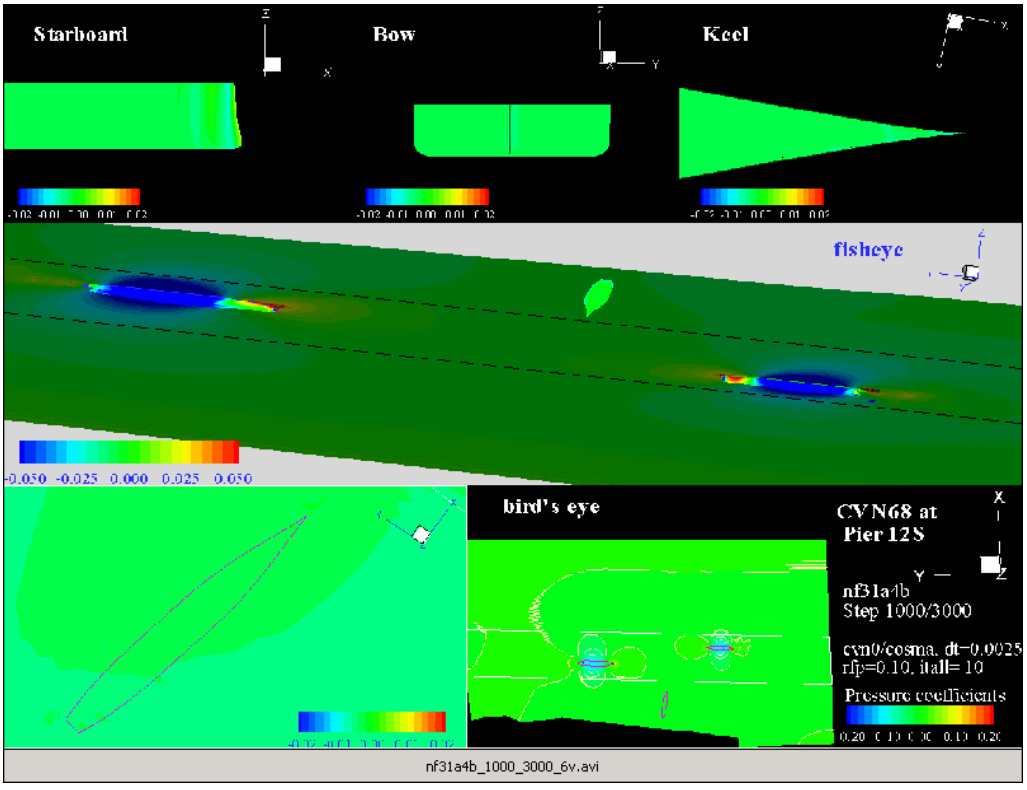

Figure 19 Motion responses of a moored ship perpendicular to the navigation channel

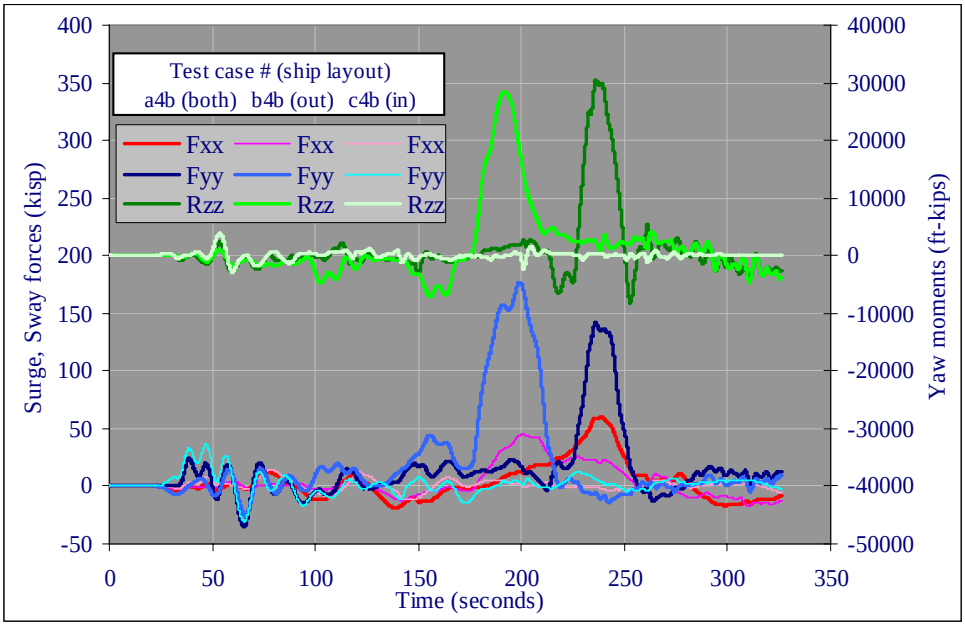

Figure 20 Fluid forces on moored ship at a real waterfront

Summaries

This paper demonstrates the merits of a modern CFD simulation model through a case study to quantify the influence of ship traffics on moored vessels in exact site environments. Simulation results enlighten the significance of site specifics to fluid activities in confined, shallow water and their consequence to ship responses. The effects are mostly introduced by basin boundaries, sea floor, ship hulls in the basin, and mooring constraints. Notable findings are recapitulated as follows.

(a) Pressure impulses induced by passing ships in shallow water decay slower over distance than the rate observed in deep water and increase much stronger than the traditional rule of speed square predicts. This is most likely due to energy being trapped in the confined depth.

(b) Reflections off vertical walls of a rectangular channel induce strong resonances in the channel. This may cause excess motions to the moored ships if an array of ships of similar size cruises by. Similar resonance, however, does not occur at a real site with irregular basin boundaries.

(c) Hydrodynamic couplings between traffic ships are significant in shallow water. The consequence affects both magnitude and phase of ship induced fluid forces. Traditional superposition method does not properly capture the total fluid forces imparted by multiple passing ships.

(d) Radiation forces on a moored ship may be as high as 50% of the corresponding excitations imposed by traffic ships. Since radiation forces are motion history dependant and fluid viscosity sensitive, a fully coupled, viscous, time-domain code is more likely to properly quantify these forces in transverse modes.

(e) Shoal water provides substantial sheltering to vessels in its shadow. Exact sea floor bathymetry is mandated to capture this effect.

Acknowledgements

This work was sponsored by Ms. Sandra Hawkinson of the Port Operations of US Naval Base Norfolk under Work Order N6268805PO001NH.

References

Chen, HC, Chen, M, and Huang, ET (1996), "Chimera RANS Simulations of Unsteady 3D Flows Induced by Ship and Structure Interactions," Flow Modeling and Turbulence Measurements VI, edited by C.J. Chen, C. Shih, J. Lienau and R.J. Kung, Balkema, Rotterdam, pp 373-380.

Chen, H.C., Chen, M. and Davis, D.A (1997), "Numerical Simulation of Transient Flows Induced by a Berthing Ship," International Journal of Offshore and Polar Engineering, Vol. 7, No. 4, pp. 277-284.

Chen, H.C., Liu, T., Huang, E.T., and Davis, D.A (2000), "Chimera RANS Simulation of Ship and Fender Coupling for Berth Operations," International Journal of Offshore and Polar Engineering, Vol. 10, No. 2, pp. 112-122.

Chen, HC and Patel, VC (1988), "Near-Wall Turbulence Models for Complex Flows Including Separation," *AIAA Journal*, Vol 26, No 6, pp. 641-648.

Suhs, NE and Tramel RW (1991), "PEGSUS 4.0 Users Manual," Arnold Engineering Development Center Report AEDC-TR-91-8, Arnold Air Force Station, TN.

Chen, H.C., Patel, V.C. and Ju, S. (1990), "Solutions of Reynolds-Averaged Navier-Stokes Equations for Three-Dimensional Incompressible Flows," Journal of Computational Physics, Vol. 88, No. 2, pp. 305-336.

Huang, T.S. (1990), "Interaction of Ships with Berth at Floating Terminals," TM-65-90-03, Naval Civil Engineering Laboratory, Port Hueneme, California.

Huang, E.T. and Chen, H.C. (2003), "Ship Berthing at a Floating Pier," Proceedings, 13th International Offshore and Polar Engineering Conference, Vol. III, pp. 683-690, Honolulu, Hawaii, May 25-30.

Chen, H.C., Liu, T., Huang, E.T., and Davis, D.A (2000), "Chimera RANS Simulation of Ship and Fender Coupling for Berth Operations," International Journal of Offshore and Polar Engineering, Vol. 10, No. 2, pp. 112-122.

Chen, H.C., Liu, T., Chang, K. and Huang, E.T., (2002), "Time-Domain Simulation of Barge Capsizing by a Chimera Domain Decomposition Approach," 12th International Offshore and Polar Engineering Conference, KitaKyushu, Japan, May 26-31